


Panoptic animal pose estimators are zero-shot performers

Shaokai Ye¹ , Alexander Mathis  , & Mackenzie Weygandt Mathis  ¹ 

¹Ecole Polytechnique Fédérale de Lausanne (EPFL), Geneva, Switzerland

 mackenzie@post.harvard.edu, alexander.mathis@epfl.ch | co-senior

Animal pose estimation is critical in applications ranging from life science research, agriculture, to veterinary medicine. Compared to human pose estimation, the performance of animal pose estimation is limited by the size of available datasets and the generalization of a model across datasets. Typically different keypoints are labeled regardless of whether the species are the same or not, leaving animal pose datasets to have disjoint or partially overlapping keypoints. As a consequence, a model cannot be used as a plug-and-play solution across datasets. This reality motivates us to develop panoptic animal pose estimation models that are able to predict keypoints defined in all datasets. In this work we propose a simple yet effective way to merge differentially labeled datasets to obtain the largest quadruped and lab mouse pose dataset. Using a gradient masking technique, so called SuperAnimal-models are able to predict keypoints that are distributed across datasets and exhibit strong zero-shot performance. The models can be further improved by (pseudo) labeled fine-tuning. These models outperform ImageNet-initialized models.

Introduction

Animal pose estimation is an important tool to study animal behavior (1–4). Compared to human pose estimation, animal pose estimation has unique challenges when it comes to dataset creation and generalization of the model to unseen animals. One major difference is that the field primarily uses animal pose estimation tools in applied, specific laboratory settings (5–10), which is in contrast to how large, diverse datasets such as how COCO and MPII are constructed, namely such that they generalize well (11, 12). This means that collectively animal datasets offer disjoint datasets, thus disjoint models, which limits the scale of datasets and the generalization ability of any one model.

For instance, images of quadrupeds such as elephants or rodents are used to train two independent models, and the images of *mus musculus* (mice) that are actually used across many laboratories are used to train targeted models within each lab, even if globally those mice look very similar and theoretically the data could be combined. Because of this practice, a model that is trained on one dataset, even though targeted to the same animal, is typically not able to generalize well, or predict unseen (yet relevant) keypoints. This lack of generalization is not due to limited model capacity, but rather the limited statistics of the training data, i.e., limited change of background, camera settings, or change of the appearance of the animal within only one experimental setting. This reality prevents animal pose estimation models from benefiting from the greatest power of deep learning methods, namely, the scalability.

To tackle this limitation, we propose **panoptic animal pose estimation models** that are able to grow by merging disjointed datasets (Figure 1). These models can predict and identify all keypoints that are defined by the collective, diverse datasets. Inspired by panoptic semantic segmenta-

tion (13), which assigns category and instance identification (ID) to every pixel in the image, we can treat animal pose estimation as a special case of panoptic semantic segmentation within the animal body, which assigns instance ID and keypoint category to every pixel if the keypoints are defined in a dataset. Although not every pixel on the body has a meaningful semantic label, as panoptic segmentation usually does, we can still safely assume that there exist more semantically meaningful keypoints on the animal body than any one animal pose dataset covers. We hypothesize a model that learns to perform panoptic pose estimation has better generalization power in both low and high(er) data regimes, and better flexibility for applied research needs.

Our proposed models benefit from diverse data and potentially learns pose features that are agnostic to the species of the animals downstream without any labeled fine-tuning. Moreover, due to its improved quality of representation, such a model could be significantly more data efficient, and thus provide better pre-training weights than commonly used ImageNet pre-trained weights (e.g., (5, 8, 14–16)).

Our contributions can be summarized as follows:

- (1) We show how to merge animal pose datasets, obtaining the largest side-view quadruped and top-view lab mice for pre-training a panoptic animal pose estimation model.
- (2) Our models have strong zero-shot performance on unseen out-of-domain (OOD) data, which can be further improved via simple pseudo-labeling in an unsupervised setting.
- (3) “SuperAnimal” models provide significantly better pre-training weights than ImageNet weights in terms of data and annotation (keypoint) efficiency.

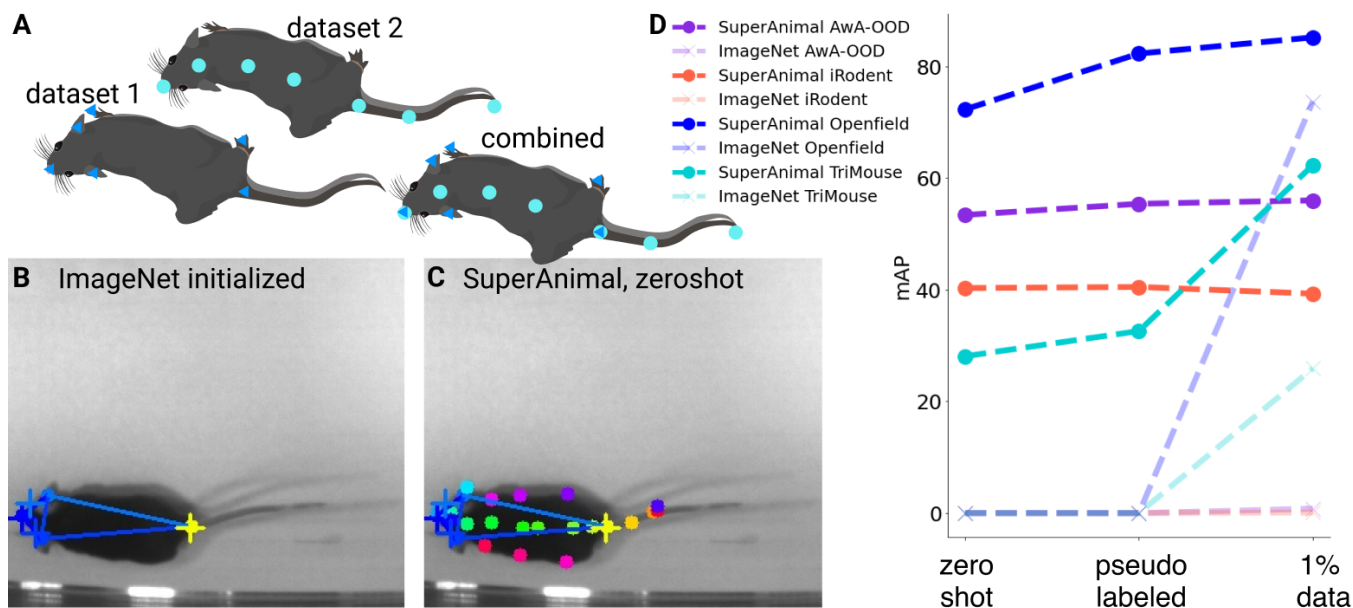


Figure 1. Panoptic animal pose estimation. (A) Often animal datasets define their own keypoints. Panoptic animal pose estimation is to predict keypoints in all datasets. (B) Predictions from a model trained on the Openfield dataset with ImageNet-initialized weights. Ground truth is marked with a cross, and model predictions are circles. Such models can only predict labels that are in the training set. (C) SuperAnimal weights are able to perform panoptic animal pose estimation: zero-shot result on an image from the held out Openfield dataset is shown. Note that more than the ground truth labels (of a given target dataset) can be predicted with SuperAnimal. Coloring as in B. (D) Results with SuperAnimal models show large gains over ImageNet-only pretraining for zero-shot, pseudo-labeling, and few-shot (i.e., 1% of the dataset, 1-8 images) settings.

Related work

Animal pose estimation. Previous works explore animal pose estimation for a large range of species in laboratory and life sciences (5–10, 17, 18). Several recent works also appeared in computer vision research, such as larger animal datasets (19–21), testing cross-domain adaptation in quadrupeds (15), out-of-distribution robustness (including cross species) and transfer learning gains with Horse-10 (22). A few papers have started to put together multi-species datasets with the same number of keypoints (with identically named labels) per animal (such as in AnimalPose and AWA (15, 19)). However, so far the benefit of merging across datasets with different keypoints, and to train a model to predict a superset of keypoints from all available datasets has not been shown. In this work, we show that such an effort creates models with strong zero-shot and fine-tuning performance.

Additionally, most (of the small set of) cross-species works have focused on non-laboratory quadrupeds (15, 19, 22, 23), while laboratory mice, who are of great importance in neuroscience and behavioral studies, have received much less attention in terms of cross-species or cross-lab animal pose estimation. To our knowledge, we are the first to provide a method to create a cross laboratory top-view mouse model, paving the way for larger efforts. For humans, DOPE (24) proposed a method to train models combining face, body and hand datasets by model distillation. However, the datasets are largely independent and rely on models trained for each dataset separately.

Pose estimation methods. Pose estimation methods can be characterized as bottom-up and top-down approaches (25, 26). In our work we demonstrate the strength of our ap-

proach for both. A top-down method uses an object detector for identifying individuals, then it’s assumed that there is one individual inside each bounding box, thus a single individual pose estimation model is applied to the cropped individual. Currently, the best methods on COCO leverage high-resolution representations (27–29). We base our work on those advances and use HRNet-w32 for top-down baselines. Bottom-up approaches do not rely on object detectors to identify individuals, and thus find all relevant keypoints and then assemble points into individuals. Different methods have been proposed (14, 29–31). Affinity-based methods such as OpenPose (30) and PifPaf (16, 32) predict the affinity between keypoints and use post processing to link keypoints of individuals. Others (29, 31) apply associative embeddings (AE) to achieve keypoint grouping. The main idea is that in addition to the category of a keypoint, the network learns to predict a cluster ID for each keypoint, and keypoints that have close cluster ID will be grouped together. Here, we use AEs with HRNets for our bottom-up baselines for their accuracy and simplicity (29).

Zero- and few-shot learning. While few-shot learning has been widely studied for classification (33–36), attribute prediction (37, 38), and detection (39–43). Yet pose estimation has received much less attention although few-shot learning is of great importance in applications (3). Early work showed that transfer learning allows for creating models in the laboratory with few annotated examples (5), and these methods are thus widely used in life sciences. WarpNet highlighted how to learn part-to-part correspondences in a weakly supervised way (44). Sanakoyeu et al. showed how to use segmentation masks, bounding boxes as well as pseudo-labeling to generalize dense-pose models to proximal animal classes (23). Sim-

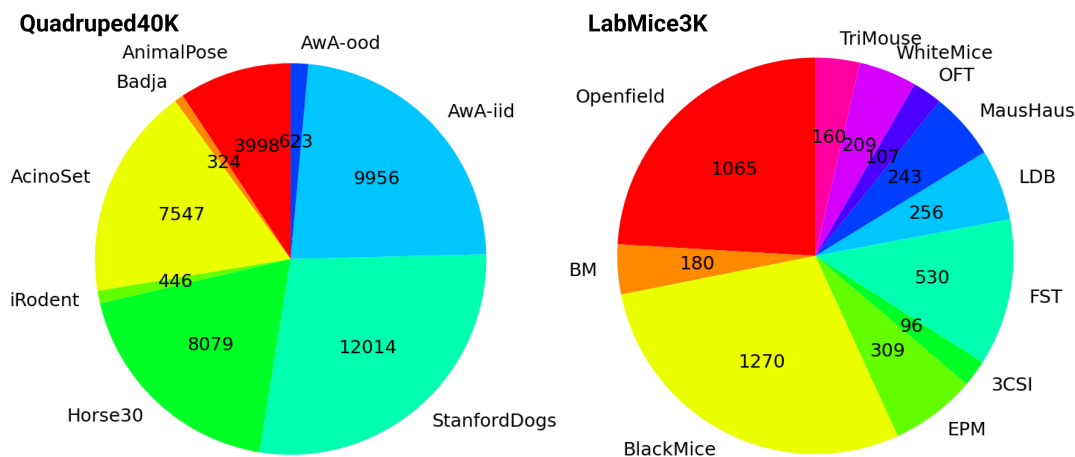


Figure 2. Dataset Composition. Left: Quadruped40K consists of 8 animal pose datasets, where two are used for ood testing (iRodent and AWA-OOD). Right: LabMice3K consists of mice data across 11 labs, where two are used for OOD testing (Openfield and TriMouse).

ilarly, Cao et al. showed how to co-train with COCO human keypoint data as well as bounding boxes and various self-supervised methods to create more robust animal pose estimation models (15), although they did not test few or zero-shot settings. Methods for few-shot 3D gaze estimation have leveraged synthetic data (45), or meta-learning for rotation invariant representations (46). Lastly, Tang et al., showed that using pose estimation can be powerful for fine-grained few-shot recognition of birds (47). Here, we are specifically interested in the few-shot learning for pose estimation.

Panoptic animal pose estimation: datasets & challenges

Here we consider animal pose estimation as performing panoptic segmentation (13) on the animal body, i.e., every pixel on the body is potentially a semantically meaningful keypoint that has an individual identity. Ideally, an infinite collection of diverse pose datasets cover all semantically meaningful keypoints and the union of keypoints that are defined across datasets make the label space of panoptic pose estimation.

Pre-training datasets. Most common animal pose data can be captured by the class quadruped (side-view point), and those of a top-view point of laboratory mice—given over 25M mice are used annually in the United States in biomedical research (48). Therefore, we combine datasets, as shown in Figure 2, that cover these two broad interest areas. Specifically, we use: StanfordDogs (21, 49), AnimalPose (15), Horse30 (22), AcinoSet (17), Badja (50), AWA (19), Openfield (51), TriMouse (52), FST-LDB-EPM-CSI-OFT (53), BlackMice (54), and in-house data.

We refer to these merged SuperAnimal datasets as “Quadruped40K” and “LabMice3K” in the following text. Each dataset has defined different number of keypoints (and naming). For our work, we used most keypoints from each individual dataset, but some are removed for simplicity in

downstream tasks (this choice does not interfere with our goals of demonstrating how to merge datasets and assess zero-shot learning performance). We held out rodents, elephants, and giraffes from the AWA dataset (19) to make an OOD test set. We also defined a main keypoint superset per SuperAnimal model in order to map dissimilarly named keypoints and non-overlapping points to the same space. For Quadruped40K we used the highest number of keypoints, which was 39 from AWA, and 26 for LabMice3K comprising 24 from MausHaus plus two additional keypoints (tailtip and headcenter) from other datasets. Thus, no specific dataset needs to be the superset. Figure 3 graphically demonstrates the mapping on the LabMice3K dataset (see Supplementary Materials for Quadruped40K).

Testing generalization: out-of-distribution datasets.

To test the generalization power (across species and laboratories) of our proposed SuperAnimal models, we focus on testing models’ performance in OOD datasets that are much harder for the models than within distribution test datasets. We ensure that the image domain of OOD datasets are very different from those of pre-training datasets.

AWA-OOD. We define this as the elephants and giraffes from the AWA dataset (19), thus splitting the original AWA dataset into AWA-IID (without elephants, rats, skunks, and giraffes) and AWA-OOD. The resulting AWA-OOD dataset has 436 training images and 187 testing images. We pick elephant and giraffe to form AWA-OOD for their rather large body size and unusual appearance compared to other quadruped animals.

iRodent. iRodent has 312 training images and 134 testing images. Rodent images were sourced from iNaturalist and labeled with 16 keypoints (from curated images of mice, rats, water rats, chipmunks). We selected this data to complement AWA-OOD (large, unusually shaped animals) to test the models’ generalization ability to small, unseen species (that often blend with the background as they are a prey species). The purpose of this is to also avoid using only AWA images in

LabMice3K Dataset creation

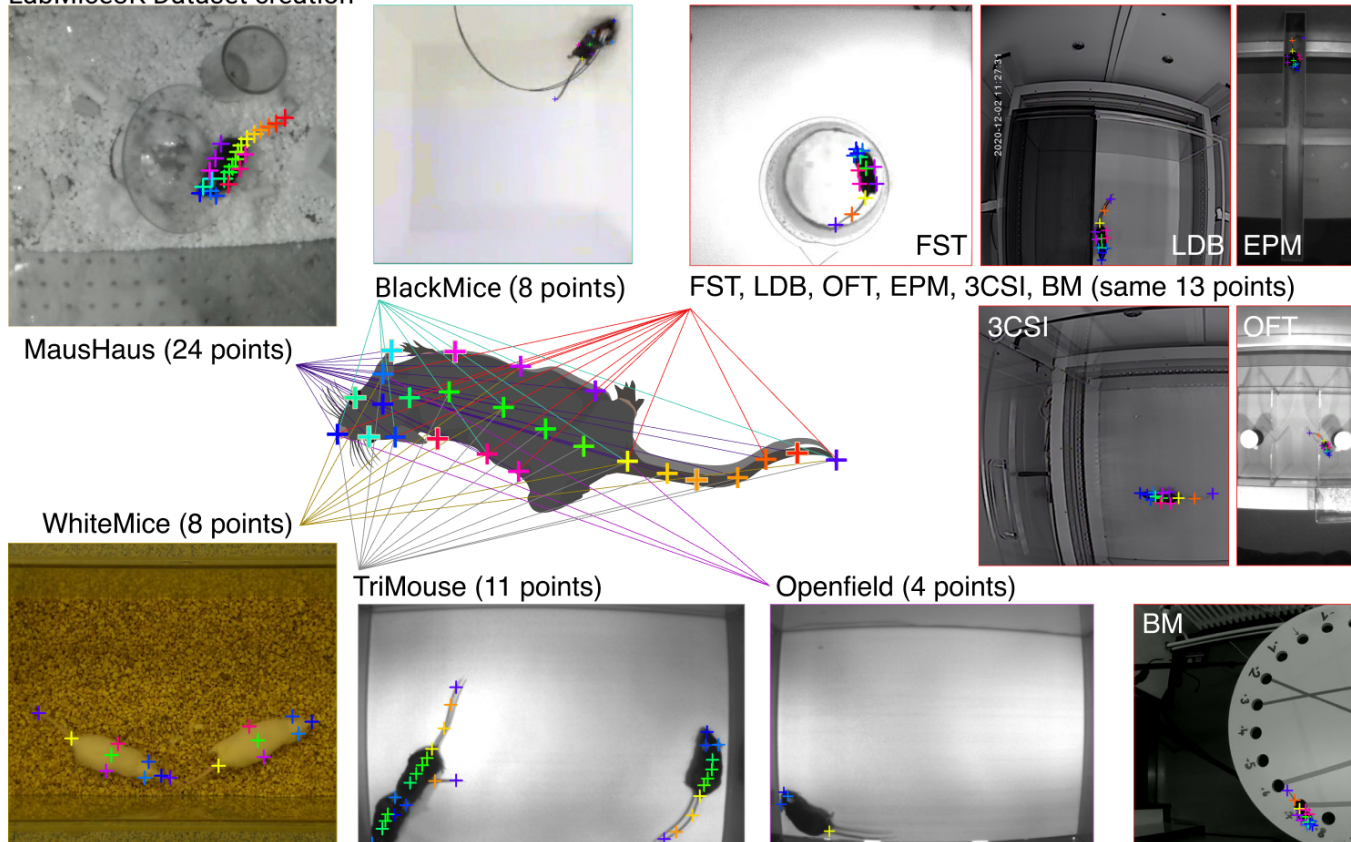


Figure 3. Merging diverse data - LabMice3K. An image (cropped for visualization clarity) of each sub-dataset with connections to mapped keypoint superset K_{\star} .

Quadruped40K-OOD.

TriMouse. TriMouse has 112 training images and 48 testing images of three mice interacting in a laboratory environment (55) and is available at (52).

Openfield. Openfield has 744 training images and 321 testing images of a single mouse in a laboratory environment (5) and is available at (51).

Merging datasets. We denote the keypoint superset K_{\star} as the union of the keypoint set for each dataset K_i :

$$K_{\star} = \bigcup_{i=1}^n K_i,$$

where n denotes the total number of datasets (Figure 2).

Oftentimes different datasets use different names for the same bodyparts (nose vs. snout, etc.), thus when merging the annotations K_i of dataset D_i we assign each keypoint to its semantically closest spot in K_{\star} . We also re-named keypoints in K_{\star} , with more details in Supplementary Materials. For those keypoints that are not originally annotated, coordinates and visibility flag (defined according to COCO convention) are left as 0s.

After projection, the keypoint annotation of every single dataset is $P \in \mathbb{R}^{2 \times m}$ where m is the total number of unique

keypoints in the superset K_{\star} . However, as the pre-training step is to learn the general representation of animal poses, the potential noise, i.e., slightly different annotations that end up being mapped to the “same” keypoint, caused by an inaccurate projection, will still allow SuperAnimal models to learn a useful representation. Automatic projection is possible and will be explored in future work.

Pose estimation models. Pose estimation aims to localize the keypoints m from image I of size $W \times H \times 3$. For the top-down methods, we utilize convolutional neural networks to regress m heatmaps of size $W/4 \times H/4$ from the high-resolution output of HRNet (28). For the bottom-up, we follow HigherHRNet, by adding an additional upsampling decoder as well as an associative embedding mechanism for keypoint grouping via tagmaps (29). The ground truth heatmaps are generated by applying a 2D Gaussian centered at the ground truth location of each keypoint. We minimize the mean square error as the loss function:

$$\mathcal{L} = \sum_{k=1}^m \sum_{i,j} \|p_k(i,j) - t_k(i,j)\|^2 \quad (1)$$

with $p_k(i,j)$ denoting the predicted heatmap and $t_k(i,j)$ the ground truth heatmap at location (i,j) .

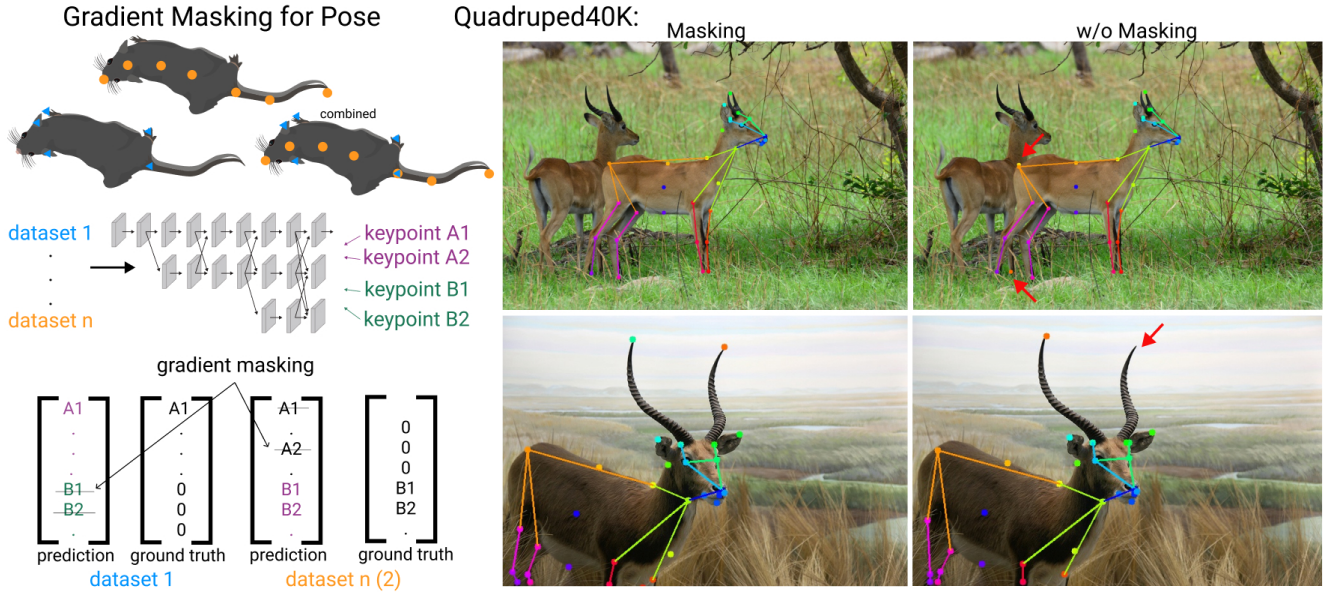


Figure 4. Gradient masking boosts performance. Left: Diagram of how gradient masking for pose estimation datasets is done. Notably, each dataset is fed into the backbone architecture, then the loss of output channels corresponding to keypoints are masked if missing from the ground truth in a given dataset to avoid penalizing missing keypoints. Right: Example test images with predictions, showing performance with and without gradient masking using the top-down method. Errors are shown by red arrows.

	Top-down	
	w/o masking	w/masking
SuperLabMice	88.4	89.5
SuperQuadruped	85.3	85.5
	Bottom-up	
	w/o masking	w/masking
SuperLabMice	82.6	86.3
SuperQuadruped	63.6	76.0

Table 1. Gradient Masking Results. 70% of the data is used to train SuperAnimal models. 30% held out data is used to report with and without gradient masking mAP.

Gradient masking. One issue with combining annotations across datasets is that some keypoints are only defined in some datasets, leaving sparse keypoint channels in the ground truth heatmaps. We found that these sparse keypoint channels can harm the performance (see Table 1). Therefore, we proposed gradient-masking, to account for unlabeled keypoints.

Specifically, we mask components of the loss across keypoints, $n_k \in \{0, 1\}$:

$$\mathcal{L} = \sum_{k=1}^m \sum_{i,j} n_k \cdot \|p_k(i,j) - t_k(i,j)\|^2 \quad (2)$$

Thereby, the keypoint mask n_k is set to 1 if the keypoint k is present in the annotation of the image and set to 0 if the keypoint is absent.

Pseudo-labeling. Although we attempt to make large, diverse datasets, it is likely the model will be impacted by domain shifts in new target tasks. To overcome this, we demonstrate that performing pseudo-labeling with the SuperAnimal models as a means of unsupervised domain adaptation can boost performance. In this work we apply pseudo-labeling as follows: we take the final coordinates of predicted keypoints (after individual identification) to fill the ground truth

annotations in a pseudo-label dataset. Note every pseudo-label annotation has visibility flag 2 (as visible and annotated in COCO) and every keypoint prediction is included (compared to high confidence filtering in (15)). After a dataset with the pseudo-label ground truth is created, we fine-tune the weights of SuperAnimals (same model weights that predict pseudo-labels) to obtain results, as shown in Table 2.

Experimental Settings

Baseline models. As we aim to provide a general solution to extend the capability of animal pose estimation models, in this work we use baseline methods that are close to state-of-the-art on the COCO keypoint estimation challenge (11) with both bottom-up and top-down approaches to demonstrate the generalization of our method.

Top-down Baselines. For top-down baselines, we used HRNet-w32 (28) with resolution 256x256. We report results for top-down baselines with ground truth bounding boxes unless stated otherwise. This is because we aim to focus on the pose estimator part of top-down baselines. Nevertheless, the animal detector is an important factor of a top-down method and the generalization of the animal detector will directly impact the top-down method. Therefore, we also trained animal

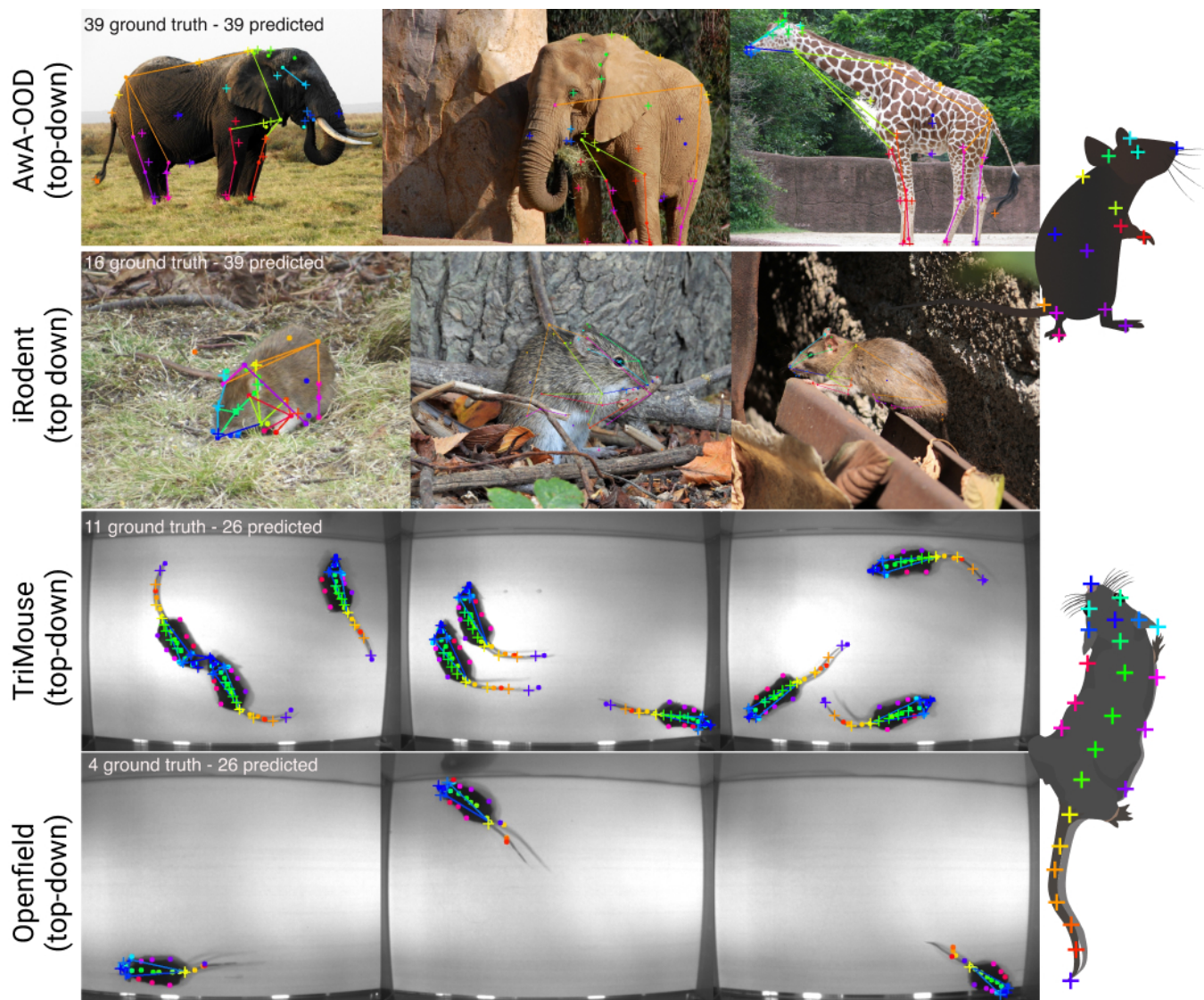


Figure 5. Zero-shot SuperAnimal pose estimation. Top Rows: Model predictions on giraffe (AwA-OOD), elephant (AwA-OOD) and rats (iRodents), which are never seen in the Quadruped40K pre-training dataset. Model predictions are denoted as dots and ground truth annotations as crosses, image inset are the maximal number of keypoints in the ground truth and predicted (but due to occlusions not all will be shown). Bottom rows: TriMouse and Openfield images that are not in the pre-training dataset. Without any labeled fine-tuning, the SuperAnimal models can accurately detect keypoints and provide reasonable detections on keypoints that are not defined in those datasets. Diagram of the maximal ground truth keypoints for each dataset is shown on the far right (side view quadruped diagram cannot visualize all).

	ImageNet	Zero-shot	Pseudo-labeling
iRodent-top-down	0	40.3	40.5
iRodent-bottom-up	0	32.4	35.8
AwA-OOD-top-down	0	53.4	55.4
AwA-OOD-bottom-up	0	47.3	51.3
Openfield-top-down	0	72.3	82.3
Openfield-bottom-up	0	61.9	67.1
TriMouse-top-down	0	28.1	32.6
TriMouse-bottom-up	0	0.2	2.1

Table 2. Zero-shot denotes model performance of SuperAnimal without any labeled fine-tuning. **Pseudo-labeling** denotes model performance of SuperAnimal models fine-tuned with pseudo-labels.

detectors using Faster R-CNN (56). Results with detectors are provided in the Supplementary Materials.

Bottom-up Baselines. Since bottom-up methods do not use an animal detector, a larger input resolution of 512x512 is used. The backbone is HRNet-w32 with one convolutional

	w/ AE weights	w/o AE weights
TriMouse-bottom-up	21.5	78.4

Table 3. Insufficiently learned associative embedding (AE) weights cause failures. SuperAnimal model fine-tuned with loading AE weights vs. SuperAnimal model fine-tuned without loading AE weights. Results are shown for SuperAnimal weights fine-tuned on TriMouse dataset with 100% training data ratio.

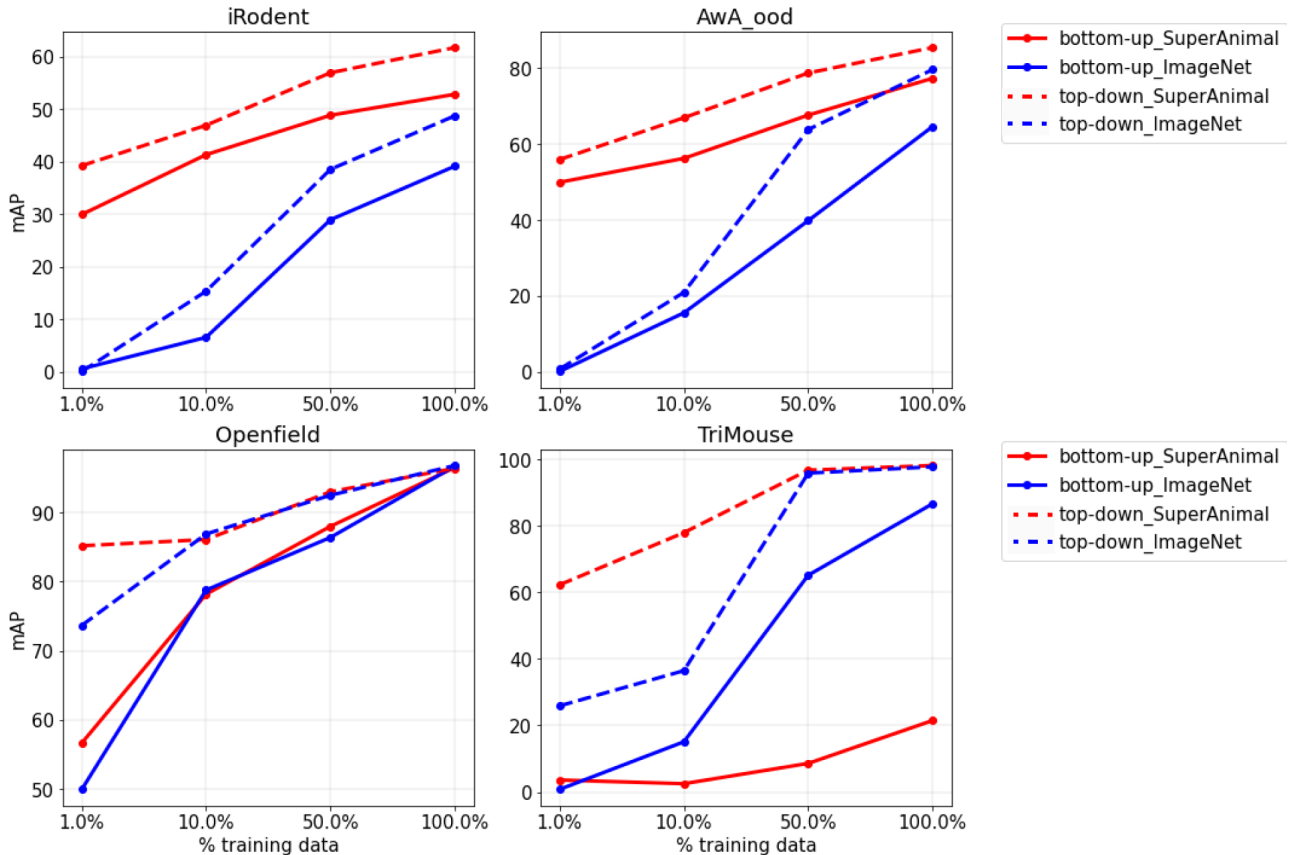


Figure 6. Models' performance with different percentage of training data. Models fine tuned with SuperAnimal weights have better performance from low data regime to high data regime, suggesting better data efficiency.

layer as the final output layer. Associative embedding is used to group keypoints into individuals (29).

Training Hyperparameters.

Top-down pose baselines. For all top-down experiments, we fix the total epochs as 210. Adam optimizer (57) is used with initial learning rate $5e-4$ and batch size 64. The learning rate is decayed by 10 at epoch 170 and 200. Warm up iteration is set to 500 and warm up ratio is set to 0.01 (58).

Bottom-up baselines. Since the bottom-up approach needs to see a whole image, making much larger input to the network, we reduce the training steps for pre-training to constrain the computational budget. In the pre-training stage, the total epoch is set to be 100 and 200 for Quadruped40K and LabMice3K respectively and Adam optimizer is used with initial learning rate $1.5e-3$. The learning rate decays by 10 at epoch 50 and 70 for Quadruped40K and at epoch 100, 160 for LabMice3K, respectively. In the fine-tuning stage, total epoch is set to be 210 with initial learning rate $1.5e-3$ for both

Quadruped40K and LabMice3K. Learning rate is decayed by 10 at epoch 160 and 200.

Pseudo-labeling. We found that pseudo-labeling does not need many training steps to reach the best performance. Therefore, a moderate learning rate $1e-4$ for Adam optimizer and early stopping at 5 epochs are used across all pseudo-labeling experiments. This low amount of training episodes are sufficient in our setting, as the well-trained SuperAnimal models are their own teacher and student and only slight modifications to the weights are required.

Evaluation Settings.

Metrics. To assess the performance we use mean average precision (mAP), a commonly used metric for pose estimation (11, 29, 55, 59). To make each keypoint equally important, we use the mean sigma from the COCO human keypoint benchmark for the Quadruped40k data. For the LabMice3K data, we assign sigma as 0.1 to every keypoint.

Heuristic Bounding Box Generation. Ground truth bounding boxes are required for both top-down baselines and mAP calculation. Therefore, for those datasets that do not have ground truth bounding boxes, we estimated them heuristically. We used the upper left keypoint and bottom right annotated keypoint of each animal to generate the initial ground truth bounding box, which is then expanded by 30 pixels.

Results

We propose a simple yet effective way to map keypoints of animal pose datasets to a superset space and merge them as if they were sparsely annotated, “super” dataset. Because the resulting dataset only contains a subset of keypoints of the superset space, their annotations become sparse after the projection and merging (up to 76% in our case). A model trained on such a dataset will experience inefficient training due to the loss between predicted dense heatmaps and the sparse ground truth heatmaps. Therefore, we propose a gradient masking method to tackle this issue. We then measure the performance of these SuperAnimal models in challenging OOD and zero-shot settings. We find that our models outperform ImageNet-only pretraining, have strong zero-shot performance, and if required, can be rapidly fine-tuned using pseudo-labeling to close the domain shift in a new target dataset.

Baseline Performance. We first assessed the within domain performance by training top-down and bottom-up models with and without gradient masking on the datasets (Table 1). We found that gradient masking always improved the results, especially for bottom-up models where a gain of up to 12 mAP could be observed. To illustrate the performance, we show predictions in Figure 4. Using gradient masking we also report the within domain (IID) performance on each dataset (see Supplementary Materials). We find that the SuperAnimal models perform well across all datasets.

Zero-shot Performance. In our setting, OOD datasets contain animal species that are not seen in the pre-training dataset, thus the models are testing whether they can generalize across species and environment, making zero-shot (testing the model without any labeled fine-tuning) a rather challenging setting. Zero-shot performance on OOD data in terms of mAP is shown in Table 2. We found large gains with SuperAnimal over ImageNet (0 vs. up to 72.3% mAP).

Models have excellent performance in challenging OOD tests (Figure 5). We also show that pseudo-labeling as a simple unsupervised domain adaptation approach (60) can increase performance on these domain shifted images. Namely, this improves the zero-shot performance with gains of 2-10% mAP (Table 2). Since the SuperAnimal models are able to predict keypoints that are not in the ground truth annotations, those keypoints cannot be evaluated. Qualitatively, we found that those predictions were accurate (Figure 5).

Data Efficiency.

Data Ratio Experiments. ImageNet weights have been shown to improve data efficiency for animal pose estimation models (5, 22). However, ImageNet weights are agnostic to the downstream task of animal pose estimation, thus likely not the best initialization weights, although they are known to be better than training from scratch (22). In this work, we aim to compare the data efficiency of ImageNet pre-training and SuperAnimal pre-training. Note that ImageNet weights are used to initialize SuperAnimal training.

Since our SuperAnimal models have been trained with a diverse set of animal pose data, the learned representation should be more robust and require less labeled data to adapt to unseen species and environments. To test whether proposed models improve data efficiency, we performed experiments to train models with 1%, 10%, and 50% of the total training data. For reference, 1% corresponds to 1 image for TriMouse, 7 images for Openfield, 4 images for AwA-OOD, and 3 images for iRodent.

SuperAnimal pretrained models largely outperform ImageNet pretrained models across datasets using both top-down and bottom-up baselines (Figure 6). For example, on iRodent with 1% of the data the models achieve an mAP of 30-40 vs 0 with ImageNet. Given enough data, for the LabMice3K OOD tests, the ImageNet methods perform on par with the SuperAnimal models. Overall, in the limit of enough data, this is expected, as even training from scratch can match training from ImageNet initialization (61).

The only notable exception is the bottom-up SuperAnimal model for the TriMouse, which performs poorly. We hypothesized this was caused by insufficiently learned associative embedding (AE) weights in our bottom-up SuperAnimal weights for LabMice3K. As shown in Figure 3, our LabMice3K pre-training dataset only includes one dataset (two white mice) that has more than one individual. Therefore, AE does not have sufficient training examples to learn how to predict embedding vectors for 3 mice in our TriMouse dataset. To test this, we design ablation study to test whether such sufficiently learned AE weights cause the failure of zero-shot setting in Table 2 and hinder the labeled fine-tuning in Figures 6, 7. As shown in Table 3, during fine-tuning, if we did not load weights from the AE layers but randomly initialize them, the performance is much better for TriMouse. This suggests that AE is not well suited for creating multiple animal pre-training models if there is not sufficient multiple individual training data in the pre-training dataset.

Sparse Keypoint Annotation Experiments. The data efficiency of our proposed models can be further tested by simulating even sparser keypoint annotations. These experiments are designed to mimic the case where the number of input images are plenty but the keypoint annotations are scarce.

We use a fixed random seed for each dataset to randomly drop 50% or 90% of the keypoint annotations from the training set. Note that these chosen keypoints are systematically dropped (i.e., the same keypoints are removed from all images) in

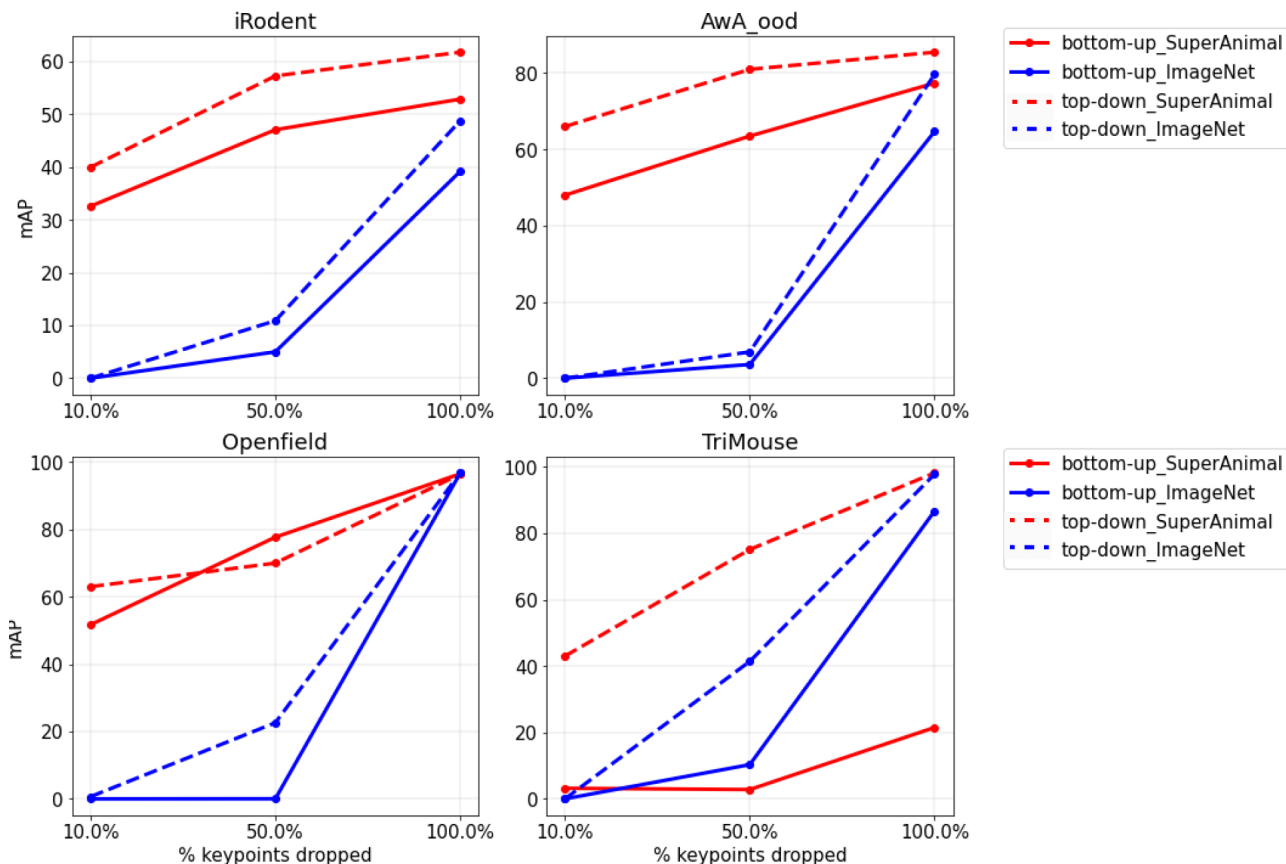


Figure 7. Sparse keypoints experiments. Up to 90% of the keypoint annotations are dropped from the training set while leaving the test set unchanged. Models fine-tuned using SuperAnimal weights largely outperform ImageNet weights because SuperAnimal weights can reason across datasets.

the training set and consistent for both bottom-up and top-down experiments. Crucially, we do not drop keypoints from the test set in order to test whether the SuperAnimal models can use knowledge learned from the pre-training datasets and potential association among keypoints to accurately predict those dropped keypoints.

We show in Figure 7 that when keypoint annotations are very sparse (90% of the keypoints are dropped), ImageNet weights have close to 0 mAP, while SuperAnimal models can still learn and even improve results upon the zero-shot setting (Figure 5). These experiments suggest that SuperAnimal models can accurately predict “dense keypoints” from sparse keypoint annotations and that the pre-training models can continue to learn to have better panoptic pose estimation performance in OOD datasets.

Conclusions

In this work we demonstrate how to merge datasets comprising diverse keypoints in order to produce SuperAnimal models that have strong zero-shot performance for all the collective keypoints on in-domain and OOD data and can be further improved by pseudo-labeling. Moreover, we show that with minimal input (less than 1% of the data, which is only 1-8 frames) from a target OOD dataset, few-shot fine-tuning boosts performance. For many conditions, SuperAnimal pre-trained models outperform ImageNet-only pre-training, thus

paving the way for better pose estimation tools in the life sciences. Furthermore, we demonstrate that one can predict labels from other datasets without any annotation of those labels. This is of great importance for downstream tasks, such as action recognition where more keypoints give better performance (62).

Acknowledgments

We are thankful to Steffen Schneider and Maxime Vidal for assistance with dataset preparation, and to Mu Zhou, Haozhe Qi, Jessy Lauer, and Linfeng Zhang for discussions, and members of the Mathis Lab and Mathis Group for comments on the manuscript. We also thank Dr. Sam Golden and Mathis Lab members for contributing unpublished data. This work was funded by a Novartis Young Investigator Award to MWM, and from EPFL. The authors declare no conflicts of interest, and the funders had no role in study design or decision to publish. We also thank scidraw.io for mouse cartoons.

Code & Data Availability

Code will be made available upon publication (within the DeepLabCut framework). Dataset citations are provided, if publicly available.

References

1. Alex Gomez-Marin, Joseph J Paton, Adam R Kampff, Rui M Costa, and Zachary F Mainen. Big behavioral data: psychology, ethology and the foundations of neuroscience. *Nature neuroscience*, 17(11): 1455, 2014.
2. Sandeep Robert Datta, David J Anderson, Kristin Branson, Pietro Perona, and Andrew Leifer. Computational neuroethology: a call to action. *Neuron*, 104(1):11–24, 2019.
3. Mackenzie Weygandt Mathis and Alexander Mathis. Deep learning tools for the measurement of animal behavior in neuroscience. *Current Opinion in Neurobiology*, 60:1–11, 2020.
4. Devis Tuia, Benjamin Kellenberger, Sara Beery, Blair R Costelloe, Silvia Zuffi, Benjamin Risse, Alexander Mathis, Mackenzie W Mathis, Frank van Langevelde, Tilo Burghardt, et al. Perspectives in machine learning for wildlife conservation. *Nature communications*, 13(1):1–15, 2022.
5. Alexander Mathis, Pranav Mamidanna, Kevin M Cury, Taiga Abe, Venkatesh N Murthy, Mackenzie Weygandt Mathis, and Matthias Bethge. Deeplabcut: markerless pose estimation of user-defined body parts with deep learning. *Nature Neuroscience*, 21(9):1281–1289, 2018.
6. Talmo D Pereira, Diego E Aldarondo, Lindsay Willmore, Mikhail Kislin, Samuel S-H Wang, Mala Murthy, and Joshua W Shaevitz. Fast animal pose estimation using deep neural networks. *Nature methods*, 16(1):117, 2019.
7. Semih Günel, Helge Rhodin, Daniel Morales, João Campagnolo, Pavan Ramdya, and Pascal Fua. Deepfly3d, a deep learning-based approach for 3d limb and appendage tracking in tethered, adult drosophila. *Elife*, 8:e48571, 2019.
8. Jacob M Graving, Daniel Chae, Hemal Naik, Liang Li, Benjamin Koger, Blair R Costelloe, and Iain D Couzin. Deepposekit, a software toolkit for fast and robust animal pose estimation using deep learning. *Elife*, 8:e47994, 2019.
9. Praneet C Bala, Benjamin R Eisenreich, Seng Bum Michael Yoo, Benjamin Y Hayden, Hyun Soo Park, and Jan Zimmermann. Automated markerless pose estimation in freely moving macaques with openmonkeystudio. *Nature communications*, 11(1):1–12, 2020.
10. Ahmet Arac, Pingping Zhao, Bruce H Dobkin, S Thomas Carmichael, and Peyman Golshani. Deepbehavior: A deep learning toolbox for automated analysis of animal and human behavior imaging data. *Frontiers in systems neuroscience*, 13:20, 2019.
11. Tsung-Yi Lin, Michael Maire, Serge Belongie, James Hays, Pietro Perona, Deva Ramanan, Piotr Dollár, and C Lawrence Zitnick. Microsoft coco: Common objects in context. In *European conference on computer vision*, pages 740–755. Springer, 2014.
12. Mykhaylo Andriiuka, Leonid Pishchulin, Peter Gehler, and Bernt Schiele. 2d human pose estimation: New benchmark and state of the art analysis. In *Proceedings of the IEEE Conference on Computer Vision and Pattern Recognition*, pages 3686–3693, 2014.
13. Alexander Kirillov, Kaiming He, Ross Girshick, Carsten Rother, and Piotr Dollár. Panoptic segmentation. In *Proceedings of the IEEE/CVF Conference on Computer Vision and Pattern Recognition*, pages 9404–9413, 2019.
14. Eldar Insafutdinov, Leonid Pishchulin, Bjoern Andres, Mykhaylo Andriiuka, and Bernt Schiele. DeeperCut: A deeper, stronger, and faster multi-person pose estimation model. In *European Conference on Computer Vision*, pages 34–50. Springer, 2016.
15. Jinkun Cao, Hongyang Tang, Hao-Shu Fang, Xiaoyong Shen, Cewu Lu, and Yu-Wing Tai. Cross-domain adaptation for animal pose estimation. In *Proceedings of the IEEE/CVF International Conference on Computer Vision*, pages 9498–9507, 2019.
16. Sven Kreiss, Lorenzo Bertoni, and Alexandre Alahi. Openpipaf: Composite fields for semantic keypoint detection and spatio-temporal association. *IEEE Transactions on Intelligent Transportation Systems*, 2021.
17. Daniel Joska, Liam Clark, Naoya Muramatsu, Ricardo Jericevich, Fred Nicolls, Alexander Mathis, Mackenzie W Mathis, and Amir Patel. Acinose: A 3d pose estimation dataset and baseline models for cheetahs in the wild. In *2021 IEEE International Conference on Robotics and Automation (ICRA)*, pages 13901–13908. IEEE, 2021.
18. Rollyn Labuguen, Jumpei Matsumoto, Salvador Blanco Negrete, Hiroshi Nishimaru, Hisao Nishijo, Masahiko Takada, Yasuhiro Go, Ken-ichi Inoue, and Tomohiro Shibata. Macaquepose: A novel “in the wild” macaque monkey pose dataset for markerless motion capture. *Frontiers in behavioral neuroscience*, page 268, 2021.
19. Prianka Banik, Lin Li, and Xishuang Dong. A novel dataset for key-point detection of quadruped animals from images. *arXiv preprint arXiv:2108.13958*, 2021.
20. Muhammad Haris Khan, John McDonagh, Salman Khan, Muhammad Shahabuddin, Aditya Arora, Fahad Shahbaz Khan, Ling Shao, and Georgios Tzimiropoulos. Animalweb: A large-scale hierarchical dataset of annotated animal faces. In *Proceedings of the IEEE/CVF Conference on Computer Vision and Pattern Recognition*, pages 6939–6948, 2020.
21. Benjamin Biggs, Oliver Boyne, James Charles, Andrew Fitzgibbon, and Roberto Cipolla. Who left the dogs out? 3d animal reconstruction with expectation maximization in the loop. In *European Conference on Computer Vision*, pages 195–211. Springer, 2020.
22. Alexander Mathis, Thomas Biasi, Steffen Schneider, Mert Yuksekogonul, Byron Rogers, Matthias Bethge, and Mackenzie W. Mathis. Pretraining boosts out-of-domain robustness for pose estimation. In *Proceedings of the IEEE/CVF Winter Conference on Applications of Computer Vision (WACV)*, pages 1859–1868, January 2021.
23. Artiom Sanakoyeu, Vasil Khalidov, Maureen S McCarthy, Andrea Vedaldi, and Natalia Neverova. Transferring dense pose to proximal animal classes. pages 5233–5242, 2020.
24. Philippe Weinzaepfel, Romain Brégier, Hadrien Combaluzier, Vincent Leroy, and Grégory Rogez. Dope: Distillation of part experts for whole-body 3d pose estimation in the wild. In *European Conference on Computer Vision*, pages 380–397. Springer, 2020.
25. Ronald Poppe. Vision-based human motion analysis: An overview. *Comput. Vis. Image Underst.*, 108:4–18, 2007.
26. Yucheng Chen, Yingli Tian, and Mingyi He. Monocular human pose estimation: A survey of deep learning-based methods. *Computer Vision and Image Understanding*, 192:102897, 2020.
27. Bin Xiao, Haiping Wu, and Yichen Wei. Simple baselines for human pose estimation and tracking. In *Proceedings of the European conference on computer vision (ECCV)*, pages 466–481, 2018.
28. Jingdong Wang, Ke Sun, Tianheng Cheng, Borui Jiang, Chaorui Deng, Yang Zhao, Dong Liu, Yadong Mu, Mingkui Tan, Xinggang Wang, et al. Deep high-resolution representation learning for visual recognition. *IEEE transactions on pattern analysis and machine intelligence*, 43(10):3349–3364, 2020.
29. Bowen Cheng, Bin Xiao, Jingdong Wang, Honghui Shi, Thomas S Huang, and Lei Zhang. Higherhrnet: Scale-aware representation learning for bottom-up human pose estimation. In *Proceedings of the IEEE/CVF Conference on Computer Vision and Pattern Recognition*, pages 5386–5395, 2020.
30. Zhe Cao, Gines Hidalgo, Tomas Simon, Shih-En Wei, and Yaser Sheikh. Openpose: Realtime multi-person 2d pose estimation using part affinity fields. arxiv 2018. *arXiv preprint arXiv:1812.08008*, 1812.
31. Alejandro Newell, Zhiao Huang, and Jia Deng. Associative embedding: End-to-end learning for joint detection and grouping. *Advances in neural information processing systems*, 30, 2017.
32. Sven Kreiss, Lorenzo Bertoni, and Alexandre Alahi. Pipaf: Composite fields for human pose estimation. In *Proceedings of the IEEE Conference on Computer Vision and Pattern Recognition*, pages 11977–11986, 2019.
33. Li Fei-Fei, Rob Fergus, and Pietro Perona. One-shot learning of object categories. *IEEE transactions on pattern analysis and machine intelligence*, 28(4):594–611, 2006.
34. Tsendsuren Munkhdalai and Hong Yu. Meta networks. In *International Conference on Machine Learning*, pages 2554–2563. PMLR, 2017.
35. Siyuan Qiao, Chenxi Liu, Wei Shen, and Alan L Yuille. Few-shot image recognition by predicting parameters from activations. In *Proceedings of the IEEE Conference on Computer Vision and Pattern Recognition*, pages 7229–7238, 2018.
36. Flood Sung, Yongxin Yang, Li Zhang, Tao Xiang, Philip HS Torr, and Timothy M Hospedales. Learning to compare: Relation network for few-shot learning. In *Proceedings of the IEEE conference on computer vision and pattern recognition*, pages 1199–1208, 2018.
37. Yongqin Xian, Christoph H Lampert, Bernt Schiele, and Zeynep Akata. Zero-shot learning—a comprehensive evaluation of the good, the bad and the ugly. *IEEE transactions on pattern analysis and machine intelligence*, 41(9):2251–2265, 2018.
38. Shubham Tulsiani, Joao Carreira, and Jitendra Malik. Pose induction for novel object categories. In *Proceedings of the IEEE International Conference on Computer Vision*, pages 64–72, 2015.
39. Jiayi Wu, Songtao Liu, Di Huang, and Yunhong Wang. Multi-scale

- positive sample refinement for few-shot object detection. In *European conference on computer vision*, pages 456–472. Springer, 2020.
40. Yang Xiao and Renaud Marlet. Few-shot object detection and viewpoint estimation for objects in the wild. In *European conference on computer vision*, pages 192–210. Springer, 2020.
 41. Bo Sun, Banghui Li, Shengcai Cai, Ye Yuan, and Chi Zhang. Fscf: Few-shot object detection via contrastive proposal encoding. In *Proceedings of the IEEE/CVF Conference on Computer Vision and Pattern Recognition*, pages 7352–7362, 2021.
 42. Zheng Ge, Songtao Liu, Zeming Li, Osamu Yoshie, and Jian Sun. Ota: Optimal transport assignment for object detection. In *Proceedings of the IEEE/CVF Conference on Computer Vision and Pattern Recognition*, pages 303–312, 2021.
 43. Weilin Zhang and Yu-Xiong Wang. Hallucination improves few-shot object detection. In *Proceedings of the IEEE/CVF Conference on Computer Vision and Pattern Recognition*, pages 13008–13017, 2021.
 44. Angjoo Kanazawa, David W Jacobs, and Manmohan Chandraker. Warpnet: Weakly supervised matching for single-view reconstruction. In *Proceedings of the IEEE Conference on Computer Vision and Pattern Recognition*, pages 3253–3261, 2016.
 45. Yu Yu, Gang Liu, and Jean-Marc Odobez. Improving few-shot user-specific gaze adaptation via gaze redirection synthesis. In *Proceedings of the IEEE/CVF Conference on Computer Vision and Pattern Recognition*, pages 11937–11946, 2019.
 46. Seonwook Park, Shalini De Mello, Pavlo Molchanov, Umar Iqbal, Otmar Hilliges, and Jan Kautz. Few-shot adaptive gaze estimation. In *Proceedings of the IEEE/CVF International Conference on Computer Vision*, pages 9368–9377, 2019.
 47. Luming Tang, Davis Wertheimer, and Bharath Hariharan. Revisiting pose-normalization for fine-grained few-shot recognition. In *Proceedings of the IEEE/CVF Conference on Computer Vision and Pattern Recognition*, pages 14352–14361, 2020.
 48. Larry Carbone. Estimating mouse and rat use in american laboratories by extrapolation from animal welfare act-regulated species. *Scientific Reports*, 11, 2021.
 49. Khosla Aditya, Jayadevaprakash Nityananda, Yao Bangpeng, and Fei-Fei Li. Novel dataset for fine-grained image categorization. In *First Workshop on Fine-Grained Visual Categorization, IEEE Conference on Computer Vision and Pattern Recognition*, 2011.
 50. Benjamin Biggs, Thomas Roddick, Andrew Fitzgibbon, and Roberto Cipolla. Creatures great and SMALL: Recovering the shape and motion of animals from video. In *ACCV*, 2018.
 51. Alexander Mathis, Pranav Mamidanna, Kevin M. Cury, Taiga Abe, Venkatesh N. Murthy, Mackenzie Weygandt Mathis, and Matthias Bethge. DeepLabCut: markerless pose estimation of user-defined body parts with deep learning. August 2018. doi: 10.5281/zenodo.4008504.
 52. Jessy Lauer, Mu Zhou, Shaokai Ye, William Menegas, Stefan Schneider, Tanmay Nath, Mohammed Mostafizur Rahman, Valentina Di Santo, Daniel Soberanes, Guoping Feng, Venkatesh N. Murthy, George Lauder, Catherine Dulac, Mackenzie Weygandt Mathis, and Alexander Mathis. madlc tri-mouse benchmark dataset - training. January 2022. doi: 10.5281/zenodo.5851157.
 53. Oliver Sturman, Lukas M. von Ziegler, Christa Schläppi, Furkan Akyol, Mattia Privitera, Daria Slominski, Christina Grimm, Laetitia Thieren, Valerio Zerbi, Benjamin F. Grewe, and Johannes Bohacek. Deep learning-based behavioral analysis reaches human accuracy and is capable of outperforming commercial solutions. *Neuropsychopharmacology*, 45:1942 – 1952, 2020.
 54. Isaac Chang. Trained DeepLabCut model for tracking mouse in open field arena with topdown view. July 2020. doi: 10.5281/zenodo.4556331.
 55. Jessy Lauer, Mu Zhou, Shaokai Ye, William Menegas, Tanmay Nath, Mohammed Mostafizur Rahman, Valentina Di Santo, Daniel Soberanes, Guoping Feng, Venkatesh N Murthy, et al. Multi-animal pose estimation and tracking with deeplabcut. *BioRxiv*, 2021.
 56. Shaoqing Ren, Kaiming He, Ross Girshick, and Jian Sun. Faster r-cnn: Towards real-time object detection with region proposal networks. *Advances in neural information processing systems*, 28, 2015.
 57. Diederik P. Kingma and Jimmy Ba. Adam: A method for stochastic optimization, 2014.
 58. Akhilesh Gotmare, Nitish Shirish Keskar, Caiming Xiong, and Richard Socher. A closer look at deep learning heuristics: Learning rate restarts, warmup and distillation. *arXiv preprint arXiv:1810.13243*, 2018.
 59. Jiefeng Li, Can Wang, Hao Zhu, Yihuan Mao, Hao-Shu Fang, and Cewu Lu. Crowdpose: Efficient crowded scenes pose estimation and a new benchmark. In *Proceedings of the IEEE Conference on Computer Vision and Pattern Recognition*, pages 10863–10872, 2019.
 60. Dong-Hyun Lee et al. Pseudo-label: The simple and efficient semi-supervised learning method for deep neural networks. In *Workshop on challenges in representation learning, ICML*, volume 3, page 896, 2013.
 61. Kaiming He, Ross Girshick, and Piotr Dollár. Rethinking imagenet pre-training. *arXiv preprint arXiv:1811.08883*, 2018.
 62. Amit Moryossef, Ioannis Tsochantaridis, Roei Aharoni, Sarah Ebling, and Sridhi Narayanan. Real-time sign language detection using human pose estimation. In *European Conference on Computer Vision*, pages 237–248. Springer, 2020.

Supplementary Material

Quadruped40K within-domain dataset. See Figure S1 for detailed information on the meaning of the keypoints for the different components of the Quadruped40K dataset.

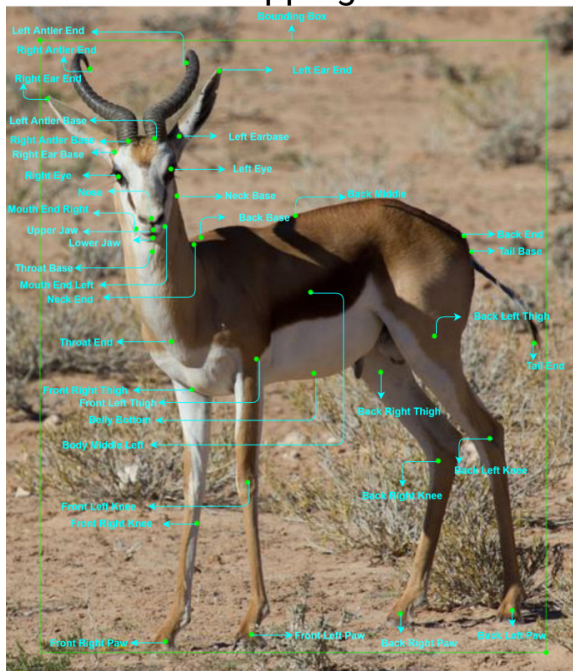
Keypoint merging across datasets. Please see Tables S1, S2 for detailed tables describing the mapping across datasets.

Impact of Inaccurate Projections. As we rely on a human expert to create the conversion table and corresponding projection rules, there could be human errors that cause inaccurate projections. In the case of LabMice3K, people usually linearly divide the spine to multiple segments. For example, in the MausHaus dataset the spine is divided into 6 segments, while in the TriMouse dataset there are 4 segments. According to our conversion table in the Appendix, spine 1 - 6 in MausHaus corresponds to neck, mid back, mouse center, mid backend, mid backend2 and mid backend 3. When it comes to the projection from 4 segments to those target keypoints in TriMouse, there could be mismatches, which might explain why zero-shot performance for TriMouse is low compared to openfield (which has no annotation on the spine). However, even based on a few training samples for the model to fine-tune, the model learns to calibrate these projection mismatch quickly as shown in Figure 6 of the main paper, going from 21.3 mAP zero-shot to 62.3 mAP with 1% training data. Future work should explore automating the process of mapping keypoint space.

Animal Detector. We used Faster R-CNN (56) to train an animal detector. The detection performance for Quadruped40K and LabMice3K respectively, is shown in Table S3. Then we tested these two detectors in their corresponding OOD datasets, as shown in row 3 to 6. We evaluated how this impacted the top-down results in the next section.

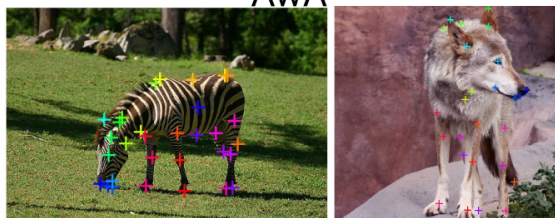
Top-down results with Detectors. We used Faster R-CNN (56) to train an animal detector. The detection performance for Quadruped40K and LabMice3K respectively, is shown in Table S3. Then we tested these two detectors in their corresponding OOD datasets, as shown in row 3 to 6.

AWA - main mapping

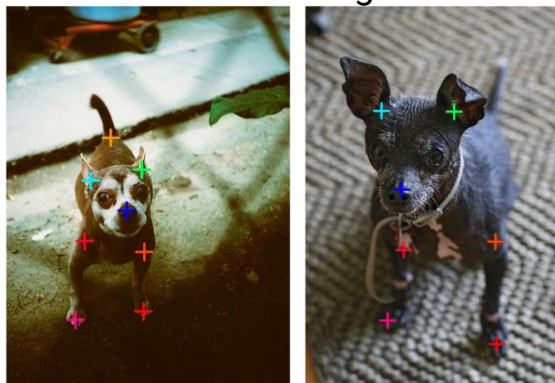


Quadruped40K-iid

AWA



StanfordDogs



AcinoSet

Horse30



AnimalPose

Badja

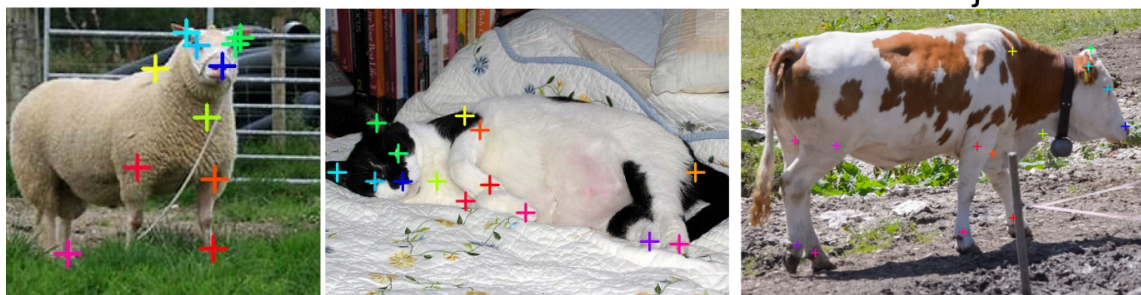


Figure S1. Examples from the datasets used to construct Quadruped40K. Top left image is adopted from AWA (19), which shows the general names of keypoints. No other dataset used this naming convention, thus we mapped into this space using animal anatomy.

We evaluated how this impacted the top-down results in the next section.

Within-domain (IID) performance baselines. In Table S5 we report the within domain performance of each individual dataset trained on each SuperAnimal model. This serves as a

reference point for the OOD datasets shown in the main paper. Note, these results are not directly comparable to any published models in the literature, as we use different train and test splits, this merely serves to highlight that within domain, SuperAnimal models achieves very high performance across multiple datasets.

Table S1. LabMice3K dataset mapping.

MausHaus	BlackMice	TriMouse	Openfield	EPM	FST	LBD	OFT	3CSI	BM	WhiteMice	MainName
nose	Nose	snout	snout	nose	nose	nose	nose	nose	nose	Nose	nose
leftearbase	Ear_left	leftear	leftear	earl	earl	earl	earl	earl	earl	Left_ear	left_ear
rightearbase	Ear_right	rightear	rightear	earr	earr	earr	earr	earr	earr	Right_ear	right_ear
righteartip											right_ear_tip
lefteye											left_eye
righteye											right_eye
spine1		shoulder		neck	neck	neck	neck	neck	neck		neck
spine2		spine1									mid_back
spine3	Center	spine2		bodycentre	bodycentre	bodycentre	bodycentre	bodycenter	bodycenter	Centroid	mouse_center
spine4		spine3									mid_backend
spine5		spine4									mid_backend2
spine6											mid_backend3
tailbase	Tail_base	tailbase	tailbase	tailbase	tailbase	tailbase	tailbase	tailbase	tailbase	Tail_base	tail_base
tail1		tail1									tail1
tail2		tail2									tail2
tail3			tailcentre	tailcentre	tailcentre	tailcentre	tailcentre	tailcenter	tailcenter		tail3
tail4											tail4
tail5											tail5
leftshoulder											left_shoulder
leftside			bcl	bcl	bcl	bcl	bcl	bcl	bcl	Left_lateral	left_midside
lefthip	Lateral_left		hipl	hipl	hipl	hipl	hipl	hipl	hipl		left_hip
rightshoulder											right_shoulder
rightside			bcr	bcr	bcr	bcr	bcr	bcr	bcr	Right_lateral	right_midside
righthip	Lateral_right		hipr	hipr	hipr	hipr	hipr	hipr	hipr		right_hip
	Tail_end	tailend	tailtip	tailtip	tailtip	tailtip	tailtip	tailtip	tailtip	Tail_end	tail_end
			headcentre	headcentre	headcentre	headcentre	headcenter	headcenter	headcenter		head_midpoint

Table S2. Quadruped40K dataset mapping.

AcinoSet	Horse30	AnimalPose	StanfordDogs	iRodent	AwA	MainName
nose	Nose	nose	Nose	nose	nose	nose
					upper_jaw	upper_jaw
					lower_jaw	lower_jaw
					mouth_end_right	mouth_end_right
					mouth_end_left	mouth_end_left
r_eye	Eye	right_eye	Right eye	right_eye	right_eye	right_eye
		right_ear	Base of Right ear	right_ear	right_earbase	right_earbase
					right_earend	right_earend
					right_antler_base	right_antler_base
					right_antler_end	right_antler_end
l_eye		left_eye	Left eye	left_ear	left_eye	left_eye
		left_ear	Base of left ear	left_ear	left_earbase	left_earbase
					left_earend	left_earend
					left_antler_base	left_antler_base
					left_antler_end	left_antler_end
neck_base					neck_base	neck_base
					neck_end	neck_end
		throat	Throat	throat	throat_base	throat_base
					throat_end	throat_end
	Wither	withers	Withers	withers	back_base	back_base
					back_end	back_end
spine					back_middle	back_middle
tail_base		tailset	Tail start	tailset	tail_base	tail_base
tail_tip					tail_end	tail_end
l_shoulder		left_front_elbow	Left front leg: top		front_left_thai	front_left_thai
l_front_knee			Left front leg: middle joint		front_left_knee	front_left_knee
l_front_paw	Nearfrontfoot	left_front_paw	Left front leg: paw	left_front_paw	front_left_paw	front_left_paw
r_shoulder	Elbow	right_front_elbow	Right front leg: top	right_front_elbow	front_right_thai	front_right_thai
r_front_knee			Right front leg: middle joint		front_right_knee	front_right_knee
r_front_paw	Offfrontfoot	right_front_paw		right_front_paw	front_right_paw	front_right_paw
l_back_paw	Offhindfoot	left_back_paw	Left rear leg: paw		back_left_paw	back_left_paw
l_hip		left_back_stifle	Left rear leg: top	left_back_stifle	back_left_thai	back_left_thai
r_hip	Stifle	right_back_stifle		right_back_stifle	back_right_thai	back_right_thai
l_back_knee			Left rear leg: middle joint		back_left_knee	back_left_knee
r_back_knee					back_right_knee	back_right_knee
r_back_paw	Nearhindfoot	right_back_paw	Right rear leg: top	right_back_paw	back_right_paw	back_right_paw
					belly_bottom	belly_bottom
					body_middle_right	body_middle_right
					body_middle_left	body_middle_left

Tested on iid validation datasets: Bounding Box AP

Quadruped40K 69

LabMice3K 70

Tested on OOD datasets:

iRodent 15

AwA-OOD 52

Openfield 3

TriMouse 16

Table S3. Average Precision (AP) for bounding boxes are reported for both IID validation set and OOD test set.

	Zero-shot	Pseudo Labeling	Fine-tuned with 100% training data
iRodent-detector	36.9	37.8	55.7
iRodent-gt	40.3	40.5	61.8
AwA-OOD-detector	50.4	56.1	84.3
AwA-OOD-gt	53.3	55.4	85.5
TriMouse-detector	24.9	25.8	96.7
TriMouse-gt	28.1	32.6	98.2
Openfield-detector	50.1	78.4	76
Openfield-gt	72.3	82.3	96.4

Table S4. Comparison of animal pose estimation with detectors and with ground truth bounding boxes (i.e., derived from GT pose estimation data)

Quadruped40K:	AnimalPose	AwA-IID	Badja	AcinoSet	Horse30	StanfordDogs			
Top-down	79.6	87.1	96.1	89.5	99.6	86.3			
Bottom-up	53.7	74.9	96.9	74.9	98.9	82			
LabMice3K:	3CSI	BlackMice	FST	MausHaus	WhiteMice	BM	EPM	LDB	OFT
Top-down	88.9	90.2	100	75.8	88.4	93.5	94	96.1	98.4
Bottom-up	92.8	95.9	100	62.7	24.4	97.1	97.5	96.2	98.6

Table S5. IID results of SuperAnimal models. Top-down results are reported with ground truth bounding boxes, reported as mAP.